Hunting for the top partner in the littlest Higgs model with T parity at the CERN LHC

Shigeki Matsumoto,* Mihoko M. Nojiri,† and Daisuke Nomura‡

Theory Group, KEK, 1-1 Oho, Tsukuba, 305-0801, Japan

(Received 5 January 2007; published 12 March 2007)

We study the littlest Higgs model with T parity at the CERN LHC through pair productions of the T-odd top quark partner (T_-) which decays into the top quark and the lightest T-odd particle. We identify the region of parameters favored by the electroweak and cosmological considerations. The signal and background events are simulated with fast detector simulation to study the discovery potential at the LHC. We find that the hemisphere analysis recently proposed by the CMS Collaboration is very useful to separate the signal from the $t\bar{t}$ background. We discuss the observability of the top tagged signal in the effective mass (M_{eff}) versus the transverse missing energy (E_{Tmiss}) plane. We show that, for all our sample parameter sets with $M_{T_-} \leq 900$ GeV, the excess of the signal over the background can be visible as a bump structure in the E_{Tmiss} distribution for 50 fb^{-1} at relatively high M_{eff} intervals.

DOI: 10.1103/PhysRevD.75.055006 PACS numbers: 14.80.Cp, 12.60.Cn, 14.65.Ha

I. INTRODUCTION

The Higgs sector in the standard model (SM) receives large quadratic mass corrections from top and gauge boson loop diagrams. New symmetries involving top-Higgs and gauge-Higgs sectors below $\mathcal{O}$ (1 TeV) are proposed to remove the corrections. One of the physics targets of the ATLAS [1] and CMS [2] experiments at the CERN LHC is to find new particles predicted by such symmetries.

The most important new physics candidate is the minimal supersymmetric standard model (MSSM)[3]. This model predicts quark and lepton partners with spin 0 (squark and slepton) and those of gauge and Higgs bosons with spin 1/2 (gauginos and Higgsinos). Thanks to the cancellation among boson and fermion loop diagrams, the quadratic corrections to the Higgs mass term completely vanish. At the LHC, strongly interacting supersymmetric particles such as a squark and a gluino will be copiously produced. They decay into relatively light electroweak (EW) superpartners, such as the chargino, neutralino, and slepton. The lightest supersymmetric particle (LSP) is stable due to the R parity of the model. The decay products of the squark and gluino contain at least one LSP. The LSP escapes from the detector without any energy deposit, giving a missing momentum signature to the events. The signature of supersymmetric particles has been studied intensively by many groups [1,2,4].

Alternative scenarios which do not rely on supersymmetry to cancel the quadratic divergent corrections have been proposed and studied. The little Higgs model [5] is one of these alternatives. In this model, the Higgs boson is regarded as a pseudo Nambu-Goldstone boson, which originates from the spontaneous breaking of a global symmetry at a certain high scale, and the global symmetry protects the Higgs mass from the quadratic radiative corrections. The simplest version of the model is called the littlest Higgs model [6]. The global symmetry of the model is SU(5), which is spontaneously broken into SO(5). Part of the SU(5) symmetry is gauged, and the gauge symmetry is $\mathrm{SU}(2)_1 \times \mathrm{SU}(2)_2 \times \mathrm{U}(1)_1 \times \mathrm{U}(1)_2$. The top sector is also extended to respect the part of the global symmetry.

This model, however, predicts a large correction to the EW observables because of the direct mixing between heavy and light gauge bosons after the EW symmetry breaking. The precision EW measurements force the masses of heavy gauge bosons and top partners to be $\mathcal{O}$ (10 TeV), reintroducing the fine-tuning problem to the Higgs mass [7]. A solution of the problem is the introduction of T parity to the model which forbids the mixing [8]. This is the symmetry under the transformations $\mathrm{SU}(2)_1 \leftrightarrow \mathrm{SU}(2)_2$ and $\mathrm{U}(1)_1 \leftrightarrow \mathrm{U}(1)_2$. All heavy gauge bosons are assigned a T-odd charge, while the SM particles have a T-even charge. The matter sector should be extended so that T-odd partners are predicted. The lightest T-odd particle is the heavy photon, which is stable and becomes a candidate for dark matter [9–11].

Starting from a different underlying theory, the littlest Higgs model with T parity ends up predicting a similar phenomenology to that of the MSSM. We view that this is indispensable for the model to remove the hierarchy problem. One needs a new symmetry to protect the Higgs mass to reduce the quadratic divergence of the theory in a meaningful manner. The symmetry must involve both the top quark and the gauge sectors, because the Higgs couplings to these particles are the dominant source of the divergences. Unless some parity is not assigned to the gauge partner, large corrections to the EW observables are expected, and those are not acceptable after the CERN LEP era. Some of the top and gauge partners are required in the parity odd sector of the model, while SM particles are in the parity even sector. Notably, if this parity is exact, the lightest parity odd particle is stable; therefore the picture is consistent with the existence of the dark matter in our Universe. Finally, the production of the top partners and

*Email address: smatsu@post.kek.jp
†Email address: nojiri@post.kek.jp
‡Email address: dnomura@post.kek.jp

their decays into the top quark and an invisible particle are predicted as the signal of "beyond the standard model" at the LHC.

For the case of the MSSM, the pair production of the scalar top is not detectable, because the production cross section is too small. Supersymmetry is instead detected by the production of gluinos and squarks in the first generation, and the scalar top may appear as the decay product of the gluino [12]. On the other hand, the cross section of the top partner pair production in the littlest Higgs model with T parity is about 10 times larger than that of the scalar top, so that they may be detectable at the LHC [13]. The purpose of this paper is to provide a realistic estimate for the detection of the fermionic top partner at the LHC.

This paper is organized as follows. In Sec. II, we review the littlest Higgs model with T parity, focusing on the top sector. In Sec. III, we summarize the electroweak and dark matter constraints on the model. We find that the lower limit of the top partner mass is about 600 GeV, and the lightest T-odd particle is always much lighter than the top partner. The signal at the LHC is therefore two top quarks with significant transverse momentum and missing energy.

In Secs. IV and V, we discuss the top partner signature at the LHC. Reconstructing a top quark in the event is essential to identify the top partner. We describe the method to reconstruct the top quark in Sec. IV. We apply a hemisphere analysis to the signal reconstruction, and study the reconstruction efficiency of the top quark for both signal and $t\bar{t}$ background. In Sec. V, we discuss the basic cuts to reduce the top quark background. The highest S/N ratio is obtained in the region where the effective mass is around twice the top partner mass. We also show the numerical results of our simulation study and find that the top partner signature would be significant over the background if the mass of the top partner is less than 1 TeV. Section VI is devoted to discussion and comments.

II. THE LITTLEST HIGGS MODEL WITH T PARITY

In this section, we briefly review the littlest Higgs model with T parity, focusing on the top sector of the model. The constraints on the model from WMAP observations and electroweak precision measurements will be discussed in the next section. For general reviews of the little Higgs models and their phenomenological aspects, see Refs. [14,15].

A. Gauge-Higgs sector

The littlest Higgs model [6] is based on a nonlinear sigma model describing an SU(5)/SO(5) symmetry breaking. The nonlinear sigma field, Σ, is given as

$$\Sigma = e^{2i\Pi/f}\Sigma_0, \tag{1}$$

where f is the vacuum expectation value associated with the breaking and is expected to be $\mathcal{O}(1)$ TeV. The Nambu-Goldstone (NG) boson matrix Π and the direction of the breaking Σ_0 are

$$\Pi = \begin{pmatrix} 0 & H/\sqrt{2} & \Phi \\ H^\dagger/\sqrt{2} & 0 & H^T/\sqrt{2} \\ \Phi^\dagger & H^*/\sqrt{2} & 0 \end{pmatrix}, \qquad \Sigma_0 = \begin{pmatrix} 0 & 0 & \mathbf{1} \\ 0 & 1 & 0 \\ \mathbf{1} & 0 & 0 \end{pmatrix}, \tag{2}$$

where we omit would-be NG fields in the Π matrix. An $[\mathrm{SU}(2)\times\mathrm{U}(1)]^2$ subgroup in the SU(5) global symmetry is gauged, which is broken down to the diagonal subgroup identified with the SM gauge group, $\mathrm{SU}(2)_L\times\mathrm{U}(1)_Y$. Because of the presence of the gauge interactions (and Yukawa interactions introduced in the next subsection), the SU(5) global symmetry is not exact, and particles in the Π matrix become pseudo NG bosons. Fourteen ($= 24 - 10$) NG bosons are decomposed into representations under the electroweak gauge group as $\mathbf{1}_0 \oplus \mathbf{3}_0 \oplus \mathbf{2}_{\pm 1/2} \oplus \mathbf{3}_{\pm 1}$. The first two representations are real, and become longitudinal components of heavy gauge bosons when the $[\mathrm{SU}(2)\times\mathrm{U}(1)]^2$ is broken down to the SM gauge group. The other scalars in the representations $\mathbf{2}_{\pm 1/2}$ and $\mathbf{3}_{\pm 1}$ are the complex doublet identified with the SM Higgs field [H in Eq. (2)] and a complex triplet Higgs field [Φ in Eq. (2)], respectively. The kinetic term of the Σ field is given as

$$\mathcal{L}_\Sigma = \frac{f^2}{8}\mathrm{Tr}[D_\mu\Sigma(D^\mu\Sigma)^\dagger], \tag{3}$$

where

$$D_\mu\Sigma = \partial_\mu\Sigma - i\sum_{j=1}^{2}[g_j(\mathbf{W}_j\Sigma + \Sigma\mathbf{W}_j^T) + g_j'(\mathbf{B}_j\Sigma + \Sigma\mathbf{B}_j^T)]. \tag{4}$$

Here, $\mathbf{W}_j = W_j^a Q_j^a$ ($\mathbf{B}_j = B_j Y_j$) is the $\mathrm{SU}(2)_j$ ($\mathrm{U}(1)_j$) gauge field and $g_j(g_j')$ is the corresponding gauge coupling constant. The generators Q_j and Y_j are

$$Q_1^a = \frac{1}{2}\begin{pmatrix} \sigma^a & 0 & 0 \\ 0 & 0 & 0 \\ 0 & 0 & 0 \end{pmatrix}, \quad Y_1 = \mathrm{diag}(3,3,-2,-2,-2)/10, \quad Q_2^a = -\frac{1}{2}\begin{pmatrix} 0 & 0 & 0 \\ 0 & 0 & 0 \\ 0 & 0 & \sigma^{a*} \end{pmatrix}, \quad Y_2 = \mathrm{diag}(2,2,2,-3,-3)/10, \tag{5}$$

where σ^a is the Pauli matrix.

In terms of the above fields, the symmetry under T parity [8] is defined as the invariance of the Lagrangian under the transformation:

$$W_1^a \leftrightarrow W_2^a, \qquad B_1 \leftrightarrow B_2,$$
$$\Pi \leftrightarrow -\Omega\Pi\Omega \text{ (or } \Sigma \leftrightarrow \tilde{\Sigma} \equiv \Sigma_0\Omega\Sigma^\dagger\Omega\Sigma_0\text{)}, \tag{6}$$

where $\Omega = \mathrm{diag}(1, 1, -1, 1, 1)$. As a result of the symmetry, the gauge coupling g_1 (g_1') must be equal to g_2 (g_2'), namely, $g_1 = g_2 = \sqrt{2}g$ ($g_1' = g_2' = \sqrt{2}g'$), where g (g') is nothing but the coupling constant of the SM $\mathrm{SU}(2)_L$ ($\mathrm{U}(1)_Y$) gauge symmetry.

The Higgs potential is generated radiatively [6,9],

$$V(H, \Phi) = \lambda f^2\,\mathrm{Tr}[\Phi^\dagger\Phi] - \mu^2 H^\dagger H + \frac{\lambda}{4}(H^\dagger H)^2 + \cdots. \tag{7}$$

The main contributions to μ^2 come from the logarithmic divergent corrections at 1-loop level and quadratic divergent corrections at 2-loop level. As a result, μ^2 is expected to be smaller than f^2. The triplet Higgs mass term, on the other hand, receives quadratic divergent corrections at 1-loop level, and therefore is proportional to f^2. The quartic coupling λ is determined by the 1-loop effective potential from the gauge and top sectors. Since both μ and λ depend on the parameters at the cutoff scale, we treat them as free parameters in this paper.

Next, we discuss the mass spectrum of the gauge and Higgs bosons. This model contains four kinds of gauge fields, W_1^a, W_2^a, B_1, and B_2, in the electroweak gauge sector. The linear combinations $W^a = (W_1^a + W_2^a)/\sqrt{2}$ and $B = (B_1 + B_2)/\sqrt{2}$ correspond to the SM gauge bosons for the $\mathrm{SU}(2)_L$ and $\mathrm{U}(1)_Y$ symmetries. The other linear combinations, $W_H^a = (W_1^a - W_2^a)/\sqrt{2}$ and $B_H = (B_1 - B_2)/\sqrt{2}$, are additional gauge bosons, which acquire masses of $\mathcal{O}(f)$ through the SU(5)/SO(5) symmetry breaking. After the electroweak symmetry breaking, the neutral components of W_H^a and B_H are mixed with each other, and form mass eigenstates A_H and Z_H. The masses of the heavy bosons are

$$m_{A_H} \simeq 0.45 g' f, \qquad m_{Z_H} \simeq m_{W_H} \simeq gf. \tag{8}$$

The mixing angle θ_H between W_H^3 and B_H is considerably suppressed. It is given by $\tan\theta_H \simeq -g'v^2/(4gf^2)$, where v ($\simeq 246$ GeV) is the vacuum expectation value of the Higgs field. Thus the dominant component of A_H is B_H. Finally, the mass of the triplet Higgs boson Φ is given by $m_\Phi^2 = \lambda f^2 = 2m_h^2 f^2/v^2$, where m_h is the SM Higgs boson mass.

Under T parity, the new heavy gauge bosons and the triplet Higgs boson behave as T-odd particles, while SM particles are T-even. As shown in Eq. (8), the heavy photon is considerably lighter than the other T-odd particles. Stability of A_H is guaranteed by T-parity conservation, and it becomes a candidate for dark matter.

B. Top sector

To implement T parity, two SU(2) doublets, q_1 and q_2, are introduced for each SM fermion doublet. Furthermore, two vectorlike singlet top partners, U_1 and U_2, are also introduced in the top sector in order to cancel large radiative corrections to the Higgs mass term. Since we are interested in top partner production at the LHC, only the top sector is discussed here. For the other matter sectors, see Refs. [9,16].

The quantum numbers of the particles in the top sector under the $[\mathrm{SU}(2) \times \mathrm{U}(1)]^2$ gauge symmetry are shown in Table I. All fields in the table are triplets under the SM $\mathrm{SU}(3)_c$ (color) symmetry. Using these fields, the Yukawa interaction terms which are invariant under T parity and gauge symmetries turn out to be

$$\mathcal{L}_t = -\frac{\lambda_1 f}{2\sqrt{2}}\epsilon_{ijk}\epsilon_{xy}[(\bar{\mathcal{Q}}_1)_i\Sigma_{jx}\Sigma_{ky} - (\bar{\mathcal{Q}}_2\Sigma_0)_i\tilde{\Sigma}_{jx}\tilde{\Sigma}_{ky}]u_R - \lambda_2 f(\bar{U}_{L1}U_{R1} + \bar{U}_{L2}U_{R2}) + \mathrm{H.c.}, \tag{9}$$

where

$$\mathcal{Q}_i = \begin{pmatrix} q_i \\ U_{Li} \\ 0 \end{pmatrix}, \qquad q_i = -\sigma^2\begin{pmatrix} u_{Li} \\ b_{Li} \end{pmatrix}. \tag{10}$$

The indices i, j, k run from 1 to 3 whereas $x, y = 4, 5$. The coupling constant λ_1 is introduced as the top Yukawa coupling, while $\lambda_2 f$ gives the vectorlike mass term for the singlet fields. Under T parity, q_i and U_i transform as $q_1 \leftrightarrow -q_2$ and $U_1 \leftrightarrow -U_2$. Therefore, the T-parity eigenstates are given by

$$q_\pm = \frac{1}{\sqrt{2}}(q_1 \mp q_2), \qquad U_{L\pm} = \frac{1}{\sqrt{2}}(U_{L1} \mp U_{L2}), \qquad U_{R\pm} = \frac{1}{\sqrt{2}}(U_{R1} \mp U_{R2}). \tag{11}$$

In terms of these eigenstates, the mass terms for these quarks are written as follows,

$$\mathcal{L}_{\mathrm{mass}} = -\lambda_1[f\bar{U}_{L+} + v\bar{u}_{L+}]u_R - \lambda_2 f(\bar{U}_{L+}U_{R+} + \bar{U}_{L-}U_{R-}) + \mathrm{H.c.} \tag{12}$$

The remaining T-odd fermion, q_-, acquires mass by introducing an additional SO(5) multiplet, transforming nonlinearly under the SU(5) symmetry. Therefore, the mass term of the q_- quark does not depend on λ_1 and λ_2. In this paper, we assume that the q_- quark is heavy compared to other top partners, and do not consider its production at the LHC. For the q_- quark phenomenology, see Refs. [16,17].

The T-even states u_+ and U_+ form the following mass eigenstates:

TABLE I. The $[\mathrm{SU}(2) \times \mathrm{U}(1)]^2$ charges for particles in the top sector.

q_1	$(\mathbf{2}, 1/30; \mathbf{1}, 2/15)$	q_2	$(\mathbf{1}, 2/15; \mathbf{2}, 1/30)$
U_{L1}	$(\mathbf{1}, 8/15; \mathbf{1}, 2/15)$	U_{L2}	$(\mathbf{1}, 2/15; \mathbf{1}, 8/15)$
U_{R1}	$(\mathbf{1}, 8/15; \mathbf{1}, 2/15)$	U_{R2}	$(\mathbf{1}, 2/15; \mathbf{1}, 8/15)$
u_R	$(\mathbf{1}, 1/3; \mathbf{1}, 1/3)$		

$$\begin{aligned} t_L &= \cos\beta u_{L+} - \sin\beta U_{L+}, \\ T_L &= \sin\beta u_{L+} + \cos\beta U_{L+}, \\ t_R &= \cos\alpha u_R - \sin\alpha U_{R+}, \\ T_R &= \sin\alpha u_R + \cos\alpha U_{R+}, \end{aligned} \tag{13}$$

where $\sin\alpha \simeq \lambda_1/(\lambda_1^2 + \lambda_2^2)^{1/2}$ and $\sin\beta \simeq \lambda_1^2 v/[(\lambda_1^2 + \lambda_2^2)f]$. The t quark is identified with the SM top quark, and T is its T-even heavy partner. On the other hand, the T-odd fermions U_{L-} and U_{R-} form a Dirac fermion, T_-. The masses of these quarks are given by

$$m_t = \frac{\lambda_1\lambda_2 v}{\sqrt{\lambda_1^2 + \lambda_2^2}}, \qquad m_T = \sqrt{\lambda_1^2 + \lambda_2^2}f, \tag{14}$$
$$m_{T_-} = \lambda_2 f.$$

It is worth noting that the T-odd states do not participate in the cancellation of quadratic divergent corrections to the Higgs mass term. The cancellation is achieved only by loop diagrams involving t and T quarks.

III. WMAP AND EW PRECISION CONSTRAINTS

In the previous section, four parameters were introduced in the gauge-Higgs and top sectors in addition to the gauge coupling constants (g and g') and the vacuum expectation value of the Higgs field (v). These are m_h, f, λ_1, and λ_2. Since the top quark mass is determined by the combination of v, λ_1, and λ_2, the number of undetermined parameters is three. These parameters can be expressed by m_h, m_{A_H}, and m_{T_-}.

In this section, we see that m_h and m_{A_H} are directly related to each other thanks to the precise data of the WMAP observations. Therefore, it is possible to write down the Higgs mass as a function of the dark matter mass, $m_h = m_h(m_{A_H})$. The electroweak precision measurements provide a further constraint on m_h and m_{T_-}. They gives a lower bound on m_{T_-} and a large mass difference between T_- and A_H.

A. Constraint from WMAP observation

First, we consider the WMAP constraint on the littlest Higgs model with T parity. The dark matter, A_H, annihilates mainly into weak gauge bosons, W^+W^- and ZZ, through diagrams in which the Higgs boson propagates in the s channel. Once we calculate the annihilation cross section, the thermal relic abundance of the dark matter is obtained by solving the Boltzmann equation. For the detailed calculation of the abundance in this model, see Refs. [9–11]. To good accuracy, the dark matter abundance can be written as

$$\Omega_{\rm DM}h^2 = 8.4 \times 10^{-2}\left(\frac{1\ {\rm pb}\cdot c}{\sigma v_{\rm rel}}\right), \tag{15}$$

where c is the speed of light, and $v_{\rm rel}$ is the relative velocity between initial dark matters. Since the product of the cross section and the relative velocity, $\sigma v_{\rm rel}$, and hence the dark matter abundance, $\Omega_{\rm DM}h^2$, depend only on m_{A_H} and m_h, the WMAP observation, $\Omega_{\rm DM}h^2 \simeq 0.111$, gives a relation between these parameters.

In Fig. 1, the thermal relic abundance of dark matter is depicted as a contour plot in the (m_{A_H}, m_h) plane. The thin shaded area is the allowed region from the WMAP observation at 2σ level, $0.094 < \Omega_{\rm DM}h^2 < 0.129$ [18]. In the figure, there are two branches: the upper branch (U branch) and the lower branch (L branch). These branches are sometimes called "low" and "high" regions, respectively [11]. In the U branch, the Higgs boson mass is larger than twice the dark matter mass, $m_h > 2m_{A_H}$, while $m_h < 2m_{A_H}$ in the L branch. The Higgs mass is precisely determined by the dark matter mass up to a twofold ambiguity by imposing the WMAP constraint.

B. Constraint from electroweak precision measurements

Next, we discuss the constraint from electroweak precision measurements. New physics contributions to electroweak observables come from radiative corrections, since there is no tree-level effect due to T parity. The constraint is sensitive to the masses of the Higgs boson and the top partner. Since the Higgs mass is directly related to the dark matter mass through the WMAP constraint, the electroweak precision constraint on m_h and m_{T_-} is translated into one on m_{A_H} and m_{T_-}.

In order to obtain the constraint, we follow the procedure in Ref. [19] using the S, T, and U parameters [20]. In that paper, it has been shown that main contributions to the parameters come from the top sector and the custodial-

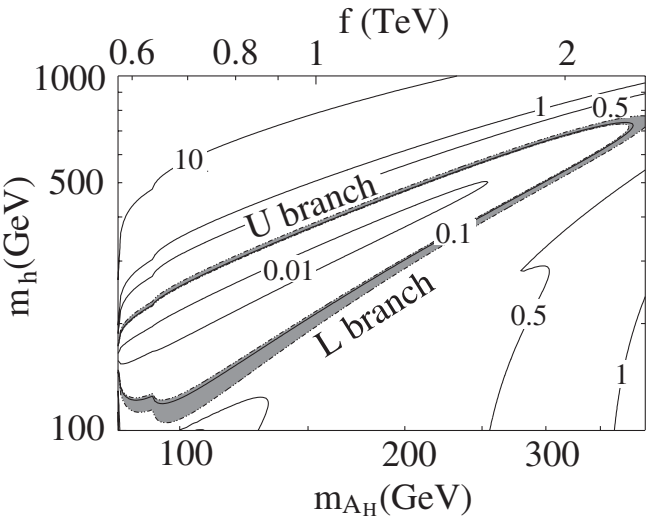

FIG. 1. Contour plot of the thermal relic abundance of the dark matter, $\Omega_{\rm DM}h^2$, in the (m_{A_H}, m_h) plane. The thin shaded area is the allowed region from the WMAP observation at 2σ level, $0.094 < \Omega_{\rm DM}h^2 < 0.129$.

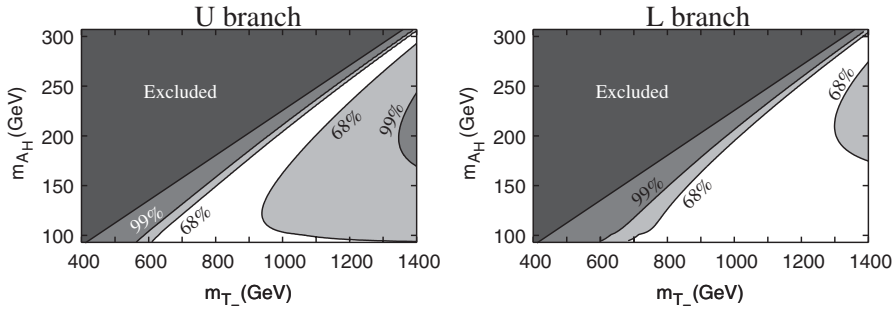

FIG. 2. Constraints on m_{T_-} and m_{A_H} at 68% and 99% confidence levels. At each point in these figures, the Higgs mass is determined to satisfy the WMAP constraint on the U branch (left panel) and L branch (right panel).

symmetry violating effect from heavy gauge boson loops. However, in Ref. [10], it has been shown that the latter contribution is negligibly small compared to the former one. Therefore, we consider only the top-sector contribution in order to obtain the constraint. For the detailed expression of the top-sector contributions, see Ref. [19].

In Fig. 2, constraints on m_{T_-} and m_{A_H} at 68% and 99% confidence levels are depicted. At each point in these figures, the Higgs mass is determined to satisfy the WMAP constraint on the U branch (left panel) and L branch (right panel). To obtain the constraint, we have used three experimental values: the W boson mass ($m_W = 80.412 \pm 0.042$ GeV), the weak mixing angle ($\sin^2\theta_{\rm eff}^{\rm lept} = 0.231\,53 \pm 0.000\,16$) [21], and the leptonic width of the Z boson ($\Gamma_l = 83.985 \pm 0.086$ MeV) [22]. We have also used the fine structure constant at the Z pole [$\alpha^{-1}(m_Z) = 128.950 \pm 0.048$] and the top quark mass ($m_t = 172.7 \pm 2.9$ GeV) [23].

As seen in these figures, the lower bound of the T_- quark mass is about 600 GeV, and the mass difference between m_{T_-} and m_{A_H} is larger than 500 GeV.[1] In the excluded region (solid black), there is no combination of the parameters λ_1, λ_2, and f which can give the correct top quark mass via Eq. (14). The parameter region with large m_{A_H} corresponds to the region with heavy m_h due to the WMAP constraint. The heavy Higgs contribution to the T parameter can be canceled by those from the top partner, T, if its mass is tuned appropriately. When $m_{A_H} \sim m_h/2$ increases, the cancellation can be achieved only for a small region of m_{T_-}, as we can see in these figures.

IV. T_- QUARK PRODUCTION AT THE LHC

In this section, we study the signature of T_- quark production at the LHC. Following the discussion in the previous section, we first discuss properties of the T_- quark and present a few representative points used in our simulation study. We next consider a top reconstruction for the signal using a hemisphere analysis. Finally, we address the background to this process, which comes from SM $t\bar{t}$ production.

A. Properties of the T_- quark

Because of the T-parity conservation, the T_- quark would be pair produced from proton-proton (pp) collisions at the LHC. Since the T_- quark has a color charge, it is produced dominantly through $\mathrm{SU}(3)_c$ interactions at the LHC. The production cross section depends only on its mass, m_{T_-}. Unlike the scalar top in the MSSM, the T_- quark is a Dirac fermion. Hence its production cross section at the LHC ranges from 0.1–1 pb when m_{T_-} is less than 1 TeV as shown in Fig. 3 (left panel).

The decay process of the T_- quark is simple, because only A_H and Z_H (W_H) are T-odd particles lighter than the T_- quark. Furthermore, the T_- quark is almost an $\mathrm{SU}(2)_L$ singlet. The interactions relevant to the decay are

$$\mathcal{L} = i\frac{2g'}{5}\cos\theta_H \bar{T}_- \not{A}_H(\sin\beta P_L + \sin\alpha P_R)t + i\frac{2g'}{5}\sin\theta_H \bar{T}_- \not{Z}_H(\sin\beta P_L + \sin\alpha P_R)t. \quad (16)$$

As seen in Eq. (16), the decay mode $T_- \to Z_H t$ is highly suppressed by $\sin^2\theta_H$; therefore T_- decays dominantly into the stable A_H and the top quark. In Fig. 3 (right panel), the decay width is depicted as a contour plot in the (m_{T_-}, m_{A_H}) plane. It shows that the width is typically several GeV.

The signal of T_- quark production is a top pair ($t\bar{t}$) with significant missing transverse momentum. In this paper, we assume that the branching ratio of the process $T_- \to A_H t$ is 100%. For simplicity we also assume that the other extra matter fermions do not contribute to the signal. The model points we choose for the simulation study are listed in Table II. The production cross sections are also shown in the table, which were obtained by the COMPHEP code [24] using the "CTEQ6L1" parton distribution function [25] and the scale of the QCD coupling set to be $Q = m_{T_-}$.

In order to generate parton level events, we calculated the process $pp \to t\bar{t}A_H A_H$ directly using the COMPHEP

[1] As shown in the previous subsection, the dominant annihilation mode of dark matter for the relic abundance is $A_H A_H \to W^+W^-$, implying that $m_{A_H} > m_W$.

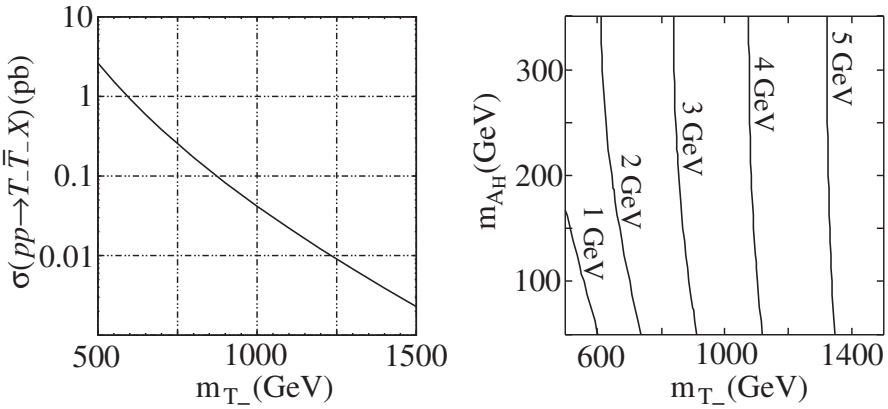

FIG. 3. Production cross section of the T_- quark at the LHC as a function of m_{T_-} (left panel). Contour plot of the T_- decay width in the (m_{T_-}, m_{A_H}) plane (right panel).

code, keeping diagrams relevant to the process through on-shell $T_-\bar{T}_-$ production. We generated 100 000 events for each model point to study their distributions. The parton level events were interfaced to HERWIG [26] for fragmentation, initial and final state radiations, and hadronization. The effect of the top polarization is not included in our simulation. The detector effects were simulated by the ACERDET code [27]. This code provides a simple detector simulation and jet reconstruction using a simple cone algorithm. It also identifies isolated leptons and photons, finds b and τ jets, and calculates the missing momentum of the events using calorimeter information.

Before going to the discussion of top reconstruction, we define two important quantities which are frequently used for new physics searches at the LHC. One is the missing transverse energy, $E_{\mathrm{Tmiss}} \equiv (P_{Tx}^2 + P_{Ty}^2)^{1/2}$, which is important for the signal of the models with a stable dark matter candidate such as the MSSM or the little Higgs model with T parity. Here P_{Ti} is the sum of transverse momenta measured by the calorimeter. The other is the effective transverse mass,

$$M_{\mathrm{eff}} \equiv \sum_{\mathrm{jets}} p_T + \sum_{\mathrm{isolated\ leptons}} p_T + \sum_{\mathrm{isolated\ photons}} p_T + E_{\mathrm{Tmiss}}, \tag{17}$$

where we require that the pseudorapidity is less than 3 ($\eta < 3$) and the transverse momentum is $p_T > 50\,(10)$ GeV for each jet (lepton/photon). The effective transverse mass is a good quantity to measure the mass scale of a produced particle.

TABLE II. The model points for our simulation study. The production cross section for the T_- quark is also shown.

	m_{T_-} (GeV)	m_{A_H} (GeV)	$\sigma(pp \to T_-\bar{T}_- + X)$ (pb)
I	600	100	0.940
II	700	125	0.382
III	800	150	0.171
IV	900	175	0.0822

B. Top reconstruction

Now we move on to the discussion of top quark reconstruction for the signal. The top quarks produced from T_- quarks have significant p_T. Since the T_- quarks must be produced in a pair, we expect two separate jet systems originating from the two top quarks. We therefore use the hemisphere analysis [28] for the event reconstruction. Two hemispheres are defined in each event, and high p_T jets, leptons, and photons are assigned to one of the hemispheres. Specifically,

(i) Each hemisphere is defined by an axis P_i ($i = 1, 2$), which is the sum of the momenta of high p_T objects (jets/leptons/photons) belonging to hemisphere i. Only the jets with $p_T > 50$ GeV and leptons/photons with $p_T > 10$ GeV are assigned to the hemisphere in order to reduce the contamination of QCD activity.

(ii) High p_T objects k belonging to hemisphere i satisfy the following condition:

$$d(p_k, P_i) < d(p_k, P_j), \tag{18}$$

where i and j are the indices of the hemispheres, and the function d is defined as

$$d(p_k, P_i) = (E_i - |P_i| \cos\theta_{ik}) \frac{E_i}{(E_i + E_k)^2}, \tag{19}$$

where θ_{ik} is the angle between P_i and p_k.

To find the axis satisfying the above conditions, we take the following steps. (1) We take the highest p_T object i (jets/leptons/photons) with momentum p_i, and the object j with the largest $\Delta R|p_j|$, where $\Delta R = [(\Delta\phi(i,j))^2 + (\Delta\eta(i,j))^2]^{1/2}$. We take p_i and p_j to be the seeds of the hemisphere axes, namely, $P_1^{\mathrm{in}} = p_i$, $P_2^{\mathrm{in}} = p_j$. (2) Each object with momentum p_k is assigned to the hemisphere i, if $d(p_k, P_i^{\mathrm{in}}) < d(p_k, P_j^{\mathrm{in}})$. (3) We then define new P_i^{in} ($i = 1, 2$) as the sum of the momenta of the objects belonging to the hemisphere i. (4) We repeat processes (2) and (3) until assignment converges. In this paper, we

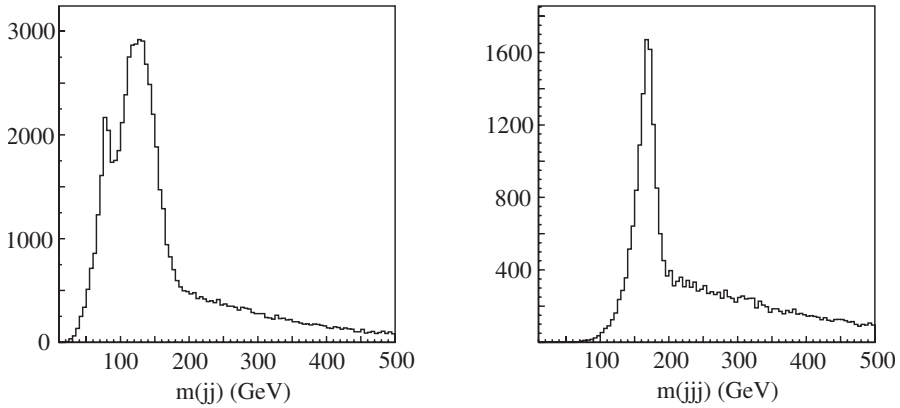

FIG. 4. Distribution of a two jet invariant mass, $m_{\max}(jj)$ (left panel), and that of $m_{\min}(jjj)$ (right panel) in the $pp \to T_-\bar{T}_- \to t\bar{t}A_HA_H$ process for point III.

denote the hemisphere seeded from the highest p_T object as "hemisphere 1" and the other as "hemisphere 2."

If there are more than two jets in a hemisphere, we can calculate the maximum of the two jet invariant masses for all combinations of jets in the hemisphere, $m_{\max}(jj)$. In Fig. 4 (left panel), we plot this for hemisphere 1 using point III in Table II. The distribution has two peaks around $m(jj) \sim 80$ GeV and 130 GeV. The lower peak corresponds to the jet pair arising from the W decay, while the second peak comes from the combination of one of the two jets from a b quark and one of the partons from the W decay.

When a hemisphere contains more than three jets, we can also define the minimum three jet invariant mass in the hemisphere, $m_{\min}(jjj)$, where two of the three jets are those which give $m_{\max}(jj)$. In Fig. 4 (right panel), the distribution peaks at the input top quark mass 175 GeV, clearly showing that the hemisphere analysis can group the jets from the top quark correctly. In the following, we often require the "top mass" cut, $m_{\min}(jjj) < 200$ GeV, for at least one of the hemispheres.

The efficiency to find at least one top quark candidate in a signal event is moderate, about 20%. In Fig. 4, we have a long tail at $m_{\min}(jjj) > 200$ GeV, which consists of events with additional jets or misassignment of jets. If we optimize the top search strategy after the hemisphere reconstruction, we may increase the top reconstruction efficiency, but we do not study this possibility in this paper. It should be noted that the reconstructed $m_{\min}(jjj)$ distribution in the hemisphere analysis is not biased, because we do not assume the existence of the top quark in the event.

C. Background

The most important background comes from the $pp \to t\bar{t} + X$ process in the SM. The tree-level production cross section of the top quark is 400 pb.[2] We have generated events corresponding to 50 fb^{-1} for this study. The cross section after very weak cuts, $M_{\rm eff} > 400$ GeV, $E_{\rm Tmiss} > 100$ GeV, $n_{\rm jets}(p_T > 100\ {\rm GeV}) \equiv n_{100} \geq 1$, and $n_{\rm jets}(p_T > 50\ {\rm GeV}) \equiv n_{50} \geq 2$, is about 16 pb, which is still higher than the signal cross section by more than a factor of 10.

The efficiency to find the top quark candidate in a hemisphere becomes lower for the $t\bar{t}$ production process if large $E_{\rm Tmiss}$ is required. This is because the W boson from the top quark decay must decay leptonically to give such a high $E_{\rm Tmiss}$ to the event. This can be seen in Table III, where we have listed the probability to find three jets with $m_{\min}(jjj) < 200$ GeV in one, or both, of the hemispheres. In Fig. 5, we present the $m_{\min}(jjj)$ distribution in a two dimensional plot, where the x (y) axis corresponds to $m_{\min}(jjj)$ in hemisphere 1 (hemisphere 2). While the distribution peaks around m_t in both of the hemispheres for the signal (left panel), the distribution for $t\bar{t}$ production scatters over the plot (right panel). This means that at least one of the top quarks has to decay leptonically, and therefore some of the jets must be additional QCD jets in $t\bar{t}$ production.

If we require a top candidate in both hemispheres, the $t\bar{t}$ background reduces to the 30 fb level; however, the reconstruction efficiency for the signal also decreases due to additional jets in the final state and the overlap of jets. In the next section, we look for the excess of signal events over the $t\bar{t}$ background for the events with $m_{\min}(jjj) < 200$ GeV in at least one of the hemispheres, for the various sample points. In this case, the $t\bar{t}$ background cross section is around 16 pb $\times$ 0.153 $\sim$ 2.5 pb, which is many orders of magnitude larger than any other irreducible backgrounds listed in [13].

In Ref. [30], it has been shown that the quark production is not the dominant background in the inclusive study of SUSY processes for the 0-lepton + $E_{\rm Tmiss}$ channel. The backgrounds from W and Z boson production are about as important as that due to $t\bar{t}$ production. However, one should be able to reduce these backgrounds significantly by

[2]The NLO cross section is 800 pb [29].

TABLE III. Fraction of $T_-\bar{T}_-$ and $t\bar{t}$ events with $m_{\rm min}(jjj) < 200$ GeV in one of the hemispheres, and in both of the hemispheres. The probability to reconstruct the top quark in both of the hemispheres is significantly small for the $t\bar{t}$ production.

	$pp \to T_-\bar{T}_-$	$pp \to t\bar{t}$
$m_{\rm min}(jjj)_1 < 200$ GeV or $m_{\rm min}(jjj)_2 < 200$ GeV	22.9%	15.3%
$m_{\rm min}(jjj)_1 < 200$ GeV and $m_{\rm min}(jjj)_2 < 200$ GeV	1.6%	0.17%

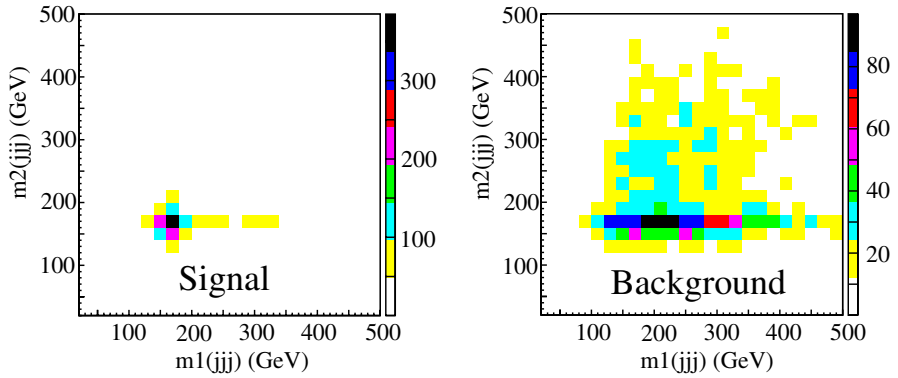

FIG. 5 (color online). Reconstructed $m_{\rm min}(jjj)$ distributions for $pp \to T_-\bar{T}_-$ for point III (left panel) and $pp \to t\bar{t}$ (right panel) processes. We take $E_{\rm Tmiss} > 400$ GeV and $n_{100} \geq 1$ and $n_{50} \geq 2$ for the $t\bar{t}$ events. The efficiency to find the top candidate in each hemisphere [$m_{\rm min}(jjj)_i < 200$ GeV] is low in the $t\bar{t}$ production compared to the signal process.

requiring a reconstructed top and b tagged jets. We therefore do not study these in this paper.

V. DISCOVERY OF THE T_- QUARK AT THE LHC

In this section, we investigate the possibility of finding the T_- quark at the LHC. First, we discuss the separation of the signal from the background using their different kinematic properties. We find the region in the $E_{\rm Tmiss}$ and $M_{\rm eff}$ plane where the signal best dominates the background. Next, we calculate the statistical significance for T_- quark discovery at the LHC, and show that the significance exceeds 7 for all sample points. We also calculate the M_{T2} variable [31] to investigate the possibility of extracting information about m_{T_-} from the signal. Finally, we comment on the differences in production and decay distributions between T_- and scalar top signals.

A. Separation of signals from backgrounds

In order to separate $T_-\bar{T}_-$ signals from $t\bar{t}$ backgrounds, we further study $E_{\rm Tmiss}$ distributions for a given (high) $M_{\rm eff}$ interval. In Fig. 6, we show the signal and background distributions in the $M_{\rm eff}$ and $E_{\rm Tmiss}$ plane. The $E_{\rm Tmiss}$ distribution of the signal peaks near its maximum ($\sim 0.5 M_{\rm eff}$) for significantly large $M_{\rm eff}$. This feature is common in processes where new particles are pair produced and each decays into a stable neutral particle and other visible particles [32]. This can be understood as follows. Since new heavy particles are produced mostly

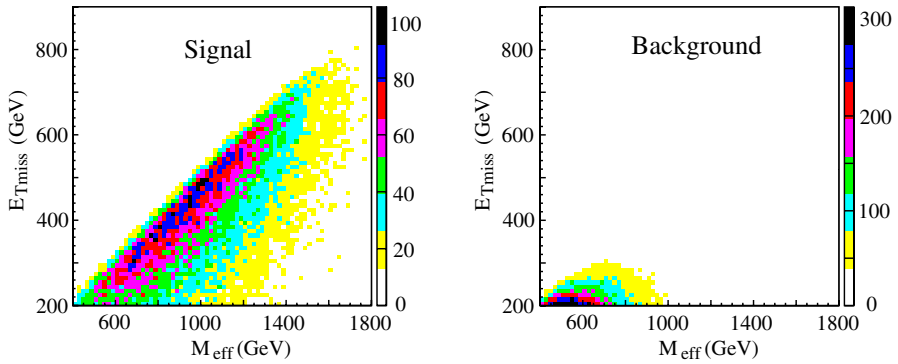

FIG. 6 (color online). $E_{\rm Tmiss}$ versus $M_{\rm eff}$ distributions for the $T_-\bar{T}_-$ production at the LHC for point III (left panel), and the $t\bar{t}$ background (right panel). Normalizations in both figures are arbitrary.

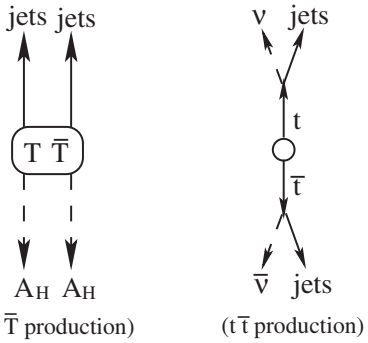

FIG. 7. $T_-\bar{T}_-$ production which gives the largest E_{Tmiss} (left panel), and background $t\bar{t}$ production with neutrino emissions.

near the threshold at the LHC, the velocity of the T_- quark is low in the transverse direction. Then, E_{Tmiss} and M_{eff} are maximized when the decay configuration of the two T_- quarks is such that the two top quarks from the decay go in the same direction in the rest frame of the $T_-\bar{T}_-$ system, as illustrated in Fig. 7. In this case, $M_{\mathrm{eff}} \sim 2E_{\mathrm{Tmiss}} \sim 2m_{T_-}$.

On the other hand, the kinematics is totally different for the background $t\bar{t}$ distribution. As shown in Fig. 7, neutrinos arising from top decays are collinear to the direction of the parent top quark, if the center of mass energy in the collision is much higher than the top quark mass. Therefore, $E_{\mathrm{Tmiss}} \sim 0.5M_{\mathrm{eff}}$ is kinematically disfavored. This can be seen in Fig. 6 (right panel). As M_{eff} increases, the fraction $E_{\mathrm{Tmiss}}/M_{\mathrm{eff}}$ is significantly reduced.

Using the nature of these production and decay kinematics, we can find the kinematical region with good separation between signal and background. We restrict M_{eff} to a certain large value, so that we see the bump of the signal event in the E_{Tmiss} distribution. In Fig. 8, we show the signal and background E_{Tmiss} distributions for points I to IV (top four panels). Each plot corresponds to the integrated luminosity $\int dt\mathcal{L} = 50\ \mathrm{fb}^{-1}$. We restrict M_{eff} to $2m_{T_-} - 200\ \mathrm{GeV} < M_{\mathrm{eff}} < 2m_{T_-}$ for $m_{T_-} = 600$ and 700 GeV, and $2m_{T_-} - 300\ \mathrm{GeV} < M_{\mathrm{eff}} < 2m_{T_-}$ for $m_{T_-} = 800$ and 900 GeV, so that E_{Tmiss} becomes maximal and the signal rate is still reasonably high. Here the top mass cut, $m_{\mathrm{min}}(jjj) < 200$ GeV, is required for at least one of the hemispheres, which reduces the background by a factor of 5 and the signal by a factor of 3 compared to the case where no cut is applied on $m_{\mathrm{min}}(jjj)$. In the bottom four panels in Fig. 8, we further require that the events have no isolated leptons. The isolated lepton is produced by the leptonic decay of the top quark. The $t\bar{t}$ background is reduced by a factor of 2 by this cut, with no significant reduction of signal events. Each distribution shows the clear excess of events over the (exponentially decreasing) background.

The excess is less prominent for smaller M_{eff} bins. We show the E_{Tmiss} distribution for point II with

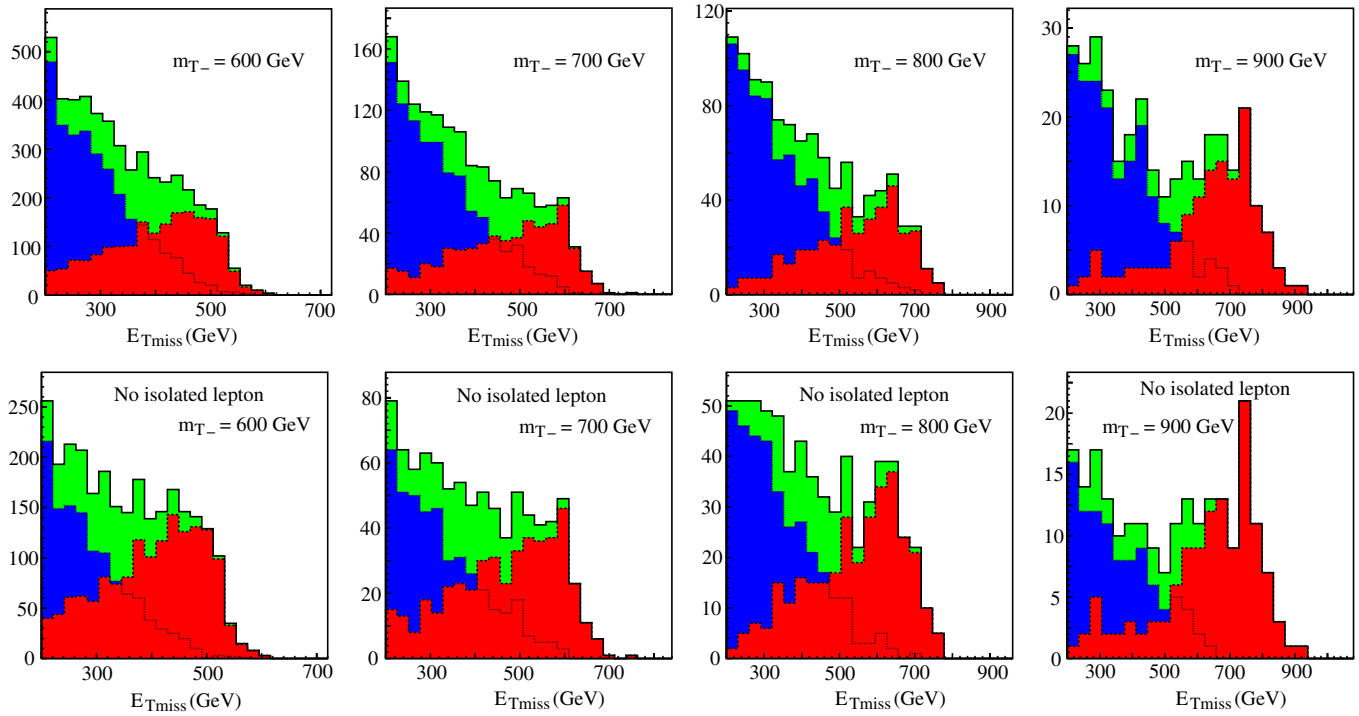

FIG. 8 (color online). E_{Tmiss} distributions for points I to IV from left to right, with $2m_{T_-} - 200\,(300)\ \mathrm{GeV} < M_{\mathrm{eff}} < 2m_{T_-}$ for $m_{T_-} \leq 700\,(\geq 800)$ GeV. The red (dark gray in the black-and-white version) and blue (darkest gray) histograms are for the signal and background distributions, and the green (light gray) histograms are the sum of these. $m_{\mathrm{min}}(jjj) < 200$ GeV is required in at least one of the hemispheres. In the bottom four panels, only the events without isolated leptons have been used.

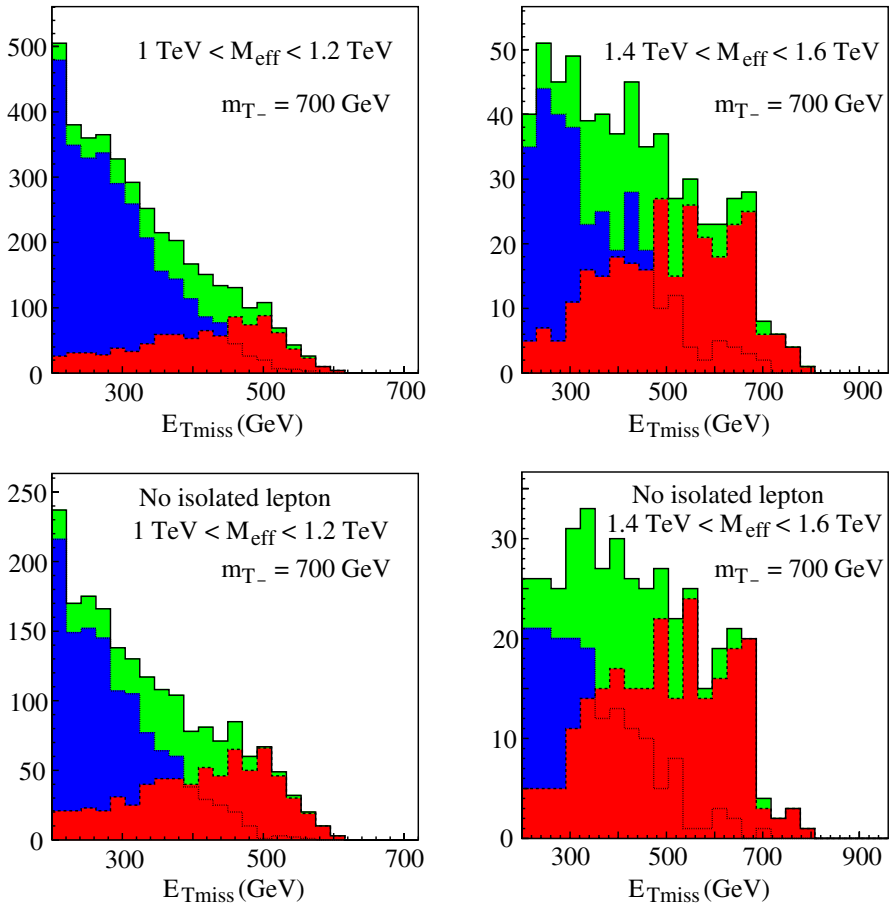

FIG. 9 (color online). E_{Tmiss} distributions for point II with 1000 GeV $< M_{\mathrm{eff}} <$ 1200 GeV (left two panels) and 1400 GeV $< M_{\mathrm{eff}} <$ 1600 GeV (right two panels). $m_{\mathrm{min}}(jjj) <$ 200 GeV is required for at least one of the hemispheres.

1000 GeV $< M_{\mathrm{eff}} <$ 1200 GeV in Fig. 9 (left two panels). While the number of the signal increases by a factor of 2, the $t\bar{t}$ background increases by more than a factor of 3. On the other hand, if one increases M_{eff}, the number of the signal reduces rather quickly, and we find that the events in this region do not contribute much to the discovery of the T_- quark. See Fig. 9 (right panel) for the distribution with 1400 GeV $< M_{\mathrm{eff}} <$ 1600 GeV. Note that the events in the region $M_{\mathrm{eff}} \gg 2m_{T_-}$ arise from highly boosted T_- quarks; therefore the fraction $E_{\mathrm{Tmiss}}/M_{\mathrm{eff}}$ decreases, making the signal distribution less prominent over the background.

The numbers of the signal and background events in the signal region are shown in Table IV. Here we take the same signal region as that of Fig. 8. The signal to background ratio with the top cut is more than 3 for all sample points. Thus, it is clearly shown that the signal dominates in the region where $E_{\mathrm{Tmiss}} \sim 0.5M_{\mathrm{eff}}$.

B. Statistical significance for the T_- quark discovery

As shown in Fig. 8, the $t\bar{t}$ background reduces rather quickly at large E_{Tmiss}. Near the end of the distribution of E_{Tmiss}, the distribution is dominated by the signal in Fig. 8. On the other hand, the signal distribution decreases quickly after its peak. We therefore fit the decrease of total distribution near the maximum value $\sim 0.5M_{\mathrm{eff}}$ to the Gaussian

TABLE IV. The signal to background ratio at sample points I to IV. We take a region with $M_{\mathrm{eff}}^{\mathrm{min}} < M_{\mathrm{eff}} < 2m_{T_-}$ and $E_{\mathrm{Tmiss}} > E_{\mathrm{Tmiss}}^{\mathrm{cut}}$. The ratio is best if one requires the top cut and vetoes isolated leptons.

m_{T_-} (GeV)	$M_{\mathrm{eff}}^{\mathrm{min}}$ (GeV)	$E_{\mathrm{Tmiss}}^{\mathrm{cut}}$ (GeV)	Signal/BG (0-lepton with top cut)	Signal/BG (with top cut)	Signal/BG
600	1000	400	842/106	1053/313	3336/1304
700	1200	450	263/54	332/114	1284/582
800	1300	500	208/28	249/57	874/417
900	1500	550	93/7	105/16	397/203

TABLE V. Fit of the E_{Tmiss} distribution to the Gaussian function near $0.5M_{\mathrm{eff}}$. Here, N_{bin} is the number of bins used for the fit and ΔE_{bin} is the bin size.

m_{T_-} (GeV)	h	Δh	σ (GeV)	N_{bin}	ΔE_{bin} (GeV)	$h/\Delta h$
600	190	14.7	38.5	7	20.8	13
700	160	6.8	43	6	25.6	24
800	46	4.9	66	6	30.4	9.4
900	17	2.4	76	6	35.2	7.1

function,

$$F(E_{\mathrm{Tmiss}}) = h\exp\left(-\frac{(E_{\mathrm{Tmiss}} - E_{\mathrm{Tmiss}}^{(\mathrm{avg})})^2}{2\sigma^2}\right). \quad (20)$$

The result is summarized in Table V, where we have used six or seven bins with the bin size (ΔE_{bin}) between 20.8 and 35.2 GeV. These fits give $\Delta\chi^2/(N_{\mathrm{bin}} - 3) \sim 1$.

The statistical significance of the signal is given by $h/\Delta h$, where h is the height of the Gaussian distribution and Δh is its error. The significance is more than 7 for all sample points. When we fit the background distribution to the same Gaussian function, we obtain $\sigma = \sigma_{t\bar{t}}$ as 102 (125) GeV for the fit above $E_{\mathrm{Tmiss}} > 304\,(328)$ GeV for 1000 GeV $< M_{\mathrm{eff}} <$ 1200 GeV (1200 GeV $< M_{\mathrm{eff}} <$ 1400 GeV), respectively. The χ^2 of the fit is $\Delta\chi^2/(N_{\mathrm{bin}} - 3) = 1.1$ (1.2). We find $\sigma \ll \sigma_{t\bar{t}}$; therefore, the detected edge is clearly inconsistent with the $t\bar{t}$ background distribution.

We found that the signal is prominent over the background when M_{eff} is restricted to the region near $2m_{T_-}$. We therefore calculate the M_{T2} variable for the events near the bump. We use "Cambridge M_{T2}," which is defined as

$$M_{T2}^2 = \min_{p_{1T}^{A_H} + p_{2T}^{A_H} = P_{\mathrm{Tmiss}}} [\max[m_{T_-}^2(p_1^{\mathrm{vis}}, p_1^{A_H}), m_{T_-}^2(p_2^{\mathrm{vis}}, p_2^{A_H})]]. \quad (21)$$

It is a function of the transverse momenta and masses of the two visible particles, P_{Tmiss}, and the mass of the invisible particle. M_{T2} is sensitive to the mass difference $m_{T_-} - m_{A_H}$, but is not sensitive to the overall mass scale. We take events where there are more than three jets with $p_T >$ 50 GeV in each hemisphere. We calculate M_{T2} by taking the visible particle momenta as the sum of the three jet momenta used to calculate the minimum three jet mass $m_{\mathrm{min}}(jjj)$ of the hemispheres, and we fix $m_{A_H} = 150$ GeV. We also require $m_{\mathrm{min}}(jjj) < 200$ GeV for at least one of the hemispheres. The distributions are shown in Fig. 10. We found a positive correlation to the mass of the top partner; however the number of events that can be used for this analysis is small.

C. Difference between T_- and scalar top signals

We discuss the differences in the production and decay distributions between the T_- quark and scalar top ($\tilde{t}$) signals. It is impossible to find the process $pp \to \tilde{t}\tilde{t}^*$ followed by the decay $\tilde{t} \to t\tilde{\chi}_1^0$ at the LHC, because the production cross section is a factor 10 smaller than the T_- quark production cross section. However, we can still learn something from the comparison.

Here we take $m_{T_-} = m_{\tilde{t}} = 800$ GeV and $m_{A_H} = m_{\tilde{\chi}_1^0} =$ 150 GeV. We took low energy parameters of the MSSM so that all particles except stop and the LSP ($\tilde{\chi}_1^0$) are too heavy to be accessible at the LHC, and $\tilde{t}$ decays into t and $\tilde{\chi}_1^0$ with a 100% branching ratio. The events for the $pp \to \tilde{t}\tilde{t}^* \to t\bar{t}\tilde{\chi}_1^0\tilde{\chi}_1^0$ process are generated by the COMPHEP code and interfaced to HERWIG.

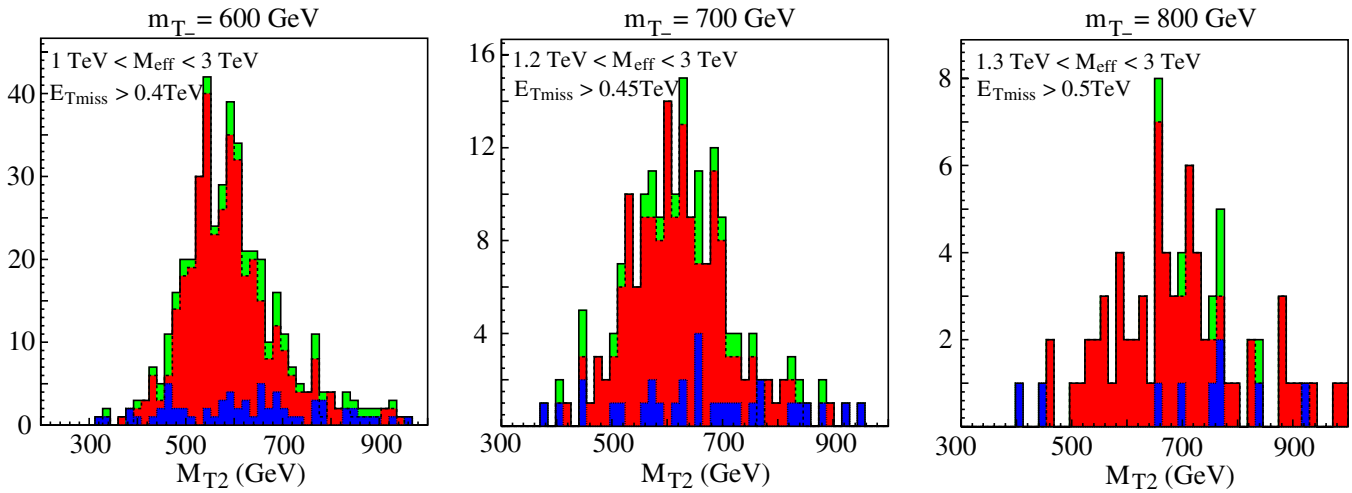

FIG. 10 (color online). Distribution of the M_{T2} variable for the events in the signal region defined in Table IV. $m_{\mathrm{min}}(jjj) < 200$ GeV is required in at least one of the hemispheres. $m_{T_-} = 600$, 700, 800 GeV from left to right.

In Fig. 11 (left panel), we show the p_T distributions of T_- and $\tilde{t}$ production at the LHC. The cross section is dominated by the low p_T component for the T_- quark. On the other hand, the $\tilde{t}$ production cross section is dominated by the P wave; therefore the p_T distribution is broadened. The production cross sections peak at 350 and 600 GeV for the T_- quark and $\tilde{t}$, respectively, where $\beta \sim 0.4$ and 0.6. Both cross sections are kinematically suppressed near the peak by β. Especially in the stop case, the squared amplitude is proportional to β^2 due to the P wave production. The cross section beyond the peak is suppressed by the quickly decreasing quark and gluon parton distribution functions. If this p_T distribution is reconstructed from the $t\bar{t}$ distribution, this indirectly suggests that the produced particle is a fermion.

The difference of the distributions affects the E_{Tmiss} distribution for fixed M_{eff} as shown in Fig. 11 (center and right panels). Here, the center panel shows the event distribution with 1300 GeV $< M_{\mathrm{eff}} <$ 1600 GeV, and, in the right panel, when the top cut is required for at least one of the hemispheres. The E_{Tmiss} distribution of the T_- events has a sharper peak near $0.5M_{\mathrm{eff}}$, while the distribution is broader for $\tilde{t}$. This is because $\tilde{t}$ is produced with higher p_T; therefore the top quark has, on average, a larger energy. Therefore the average fraction $E_{\mathrm{Tmiss}}/M_{\mathrm{eff}}$ becomes smaller.

Finally we comment on the top reconstruction for the supersymmetric signature. In supersymmetric models, the top quarks mostly arise from gluino decays through processes $\tilde{g} \to \tilde{t}t$, $\tilde{g} \to \tilde{b}b \to tb\tilde{\chi}^+$. The top quark in the event is hardly seen in the $m_{\mathrm{min}}(jjj)$ distribution due to the additional high p_T jets and leptons. In previous studies, the top quark is therefore searched for by looking for the jets consistent with the top decay kinematics, namely, $m(jj) \sim 80$ GeV and $m(bjj) \sim 175$ GeV by looking for the combination of jets i, j, and k, which minimizes $\Delta\chi^2$ defined as

$$\Delta\chi^2 = \frac{(m(i,j) - m_W)^2}{(\Delta m_W)^2} + \frac{(m(i,j,k) - m_t)^2}{(\Delta m_t)^2}, \qquad (22)$$

where Δm_W and Δm_t are the expected errors on W and top mass reconstruction.

The efficiency to find the top quark in the events becomes higher if we look for the jet combination consistent with top decay kinematics; however, in this case, we occasionally find top candidates in events which do not contain parton level top quarks, increasing backgrounds from the other SM processes [33]. The signal distributions may also be distorted by such a procedure. This is particularly the case when the number of jets in the events is large. A scheme to subtract the accidental background from the top decay kinematical distributions has been developed [12].

VI. DISCUSSION AND OUTLOOK

In this paper, we have studied the phenomenology of the top partner in the littlest Higgs model with T parity. This model predicts a stable neutral massive gauge boson (A_H), and a relatively light top partner (T_-). The EW precision measurements and dark matter observations constrain parameters of the model, f, m_h, λ_1, and λ_2. We find m_{A_H} and m_h are strongly constrained by the relic density constraint, if coannihilation processes with other T-odd particles are not efficient. Combined with the EW precision measurements, we have found the lower limit of m_{T_-} as a function of f, and clarified the fact that the top partner mass must be above 600 GeV, and the mass difference between T_- and A_H is large. The signature of T_- quark pair production at the LHC is therefore high p_T top quarks from $T_- \to tA_H$

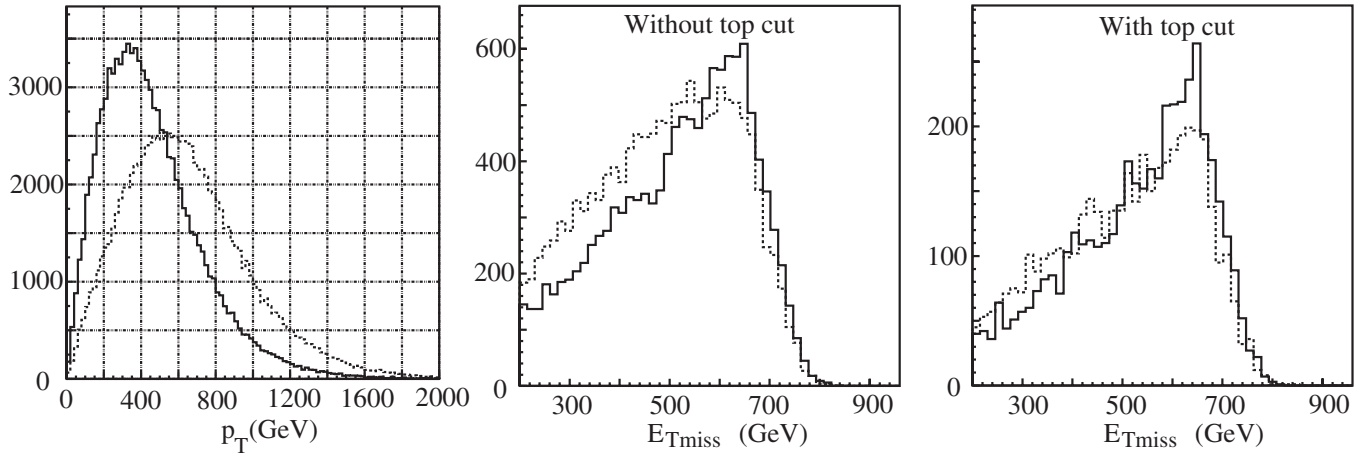

FIG. 11. The p_T distribution of T_- (solid line) and $\tilde{t}$ (dashed line) at the LHC (left panel). The 10^5 events are generated by the COMPHEP code. We set $m_{T_-} = m_{\tilde{t}} = 800$ GeV. The E_{Tmiss} distribution for T_- (solid line) and $\tilde{t}$ (dashed line) productions with 1300 GeV $< M_{\mathrm{eff}} <$ 1600 GeV (center and right panels). For the right panel, we required $m_{\mathrm{min}}(jjj) < 200$ GeV for at least one of the hemispheres.

and missing p_T coming from the A_H. We have studied the signal and background distributions at the LHC.

Unbiased reconstruction of the top quark is essential to establish the existence of the top partner without increasing accidental backgrounds. We apply the hemisphere analysis, which is an algorithm to find two axes in events originating from particles produced in pairs. We have found that the appropriately defined three jet invariant mass in a hemisphere shows a clear peak at the top quark mass with a tail due to misreconstructed events. The three jet invariant mass is calculated from the pair of jets giving the maximum invariant mass in a hemisphere and a jet giving the minimum three jet invariant mass when combined with this jet pair. The efficiency to reconstruct at least one top quark, i.e. a hemisphere with $m_{\min}(jjj) <$ 200 GeV in $T_-\bar{T}_-$ events, is reasonable, $\sim$20%.

The dominant background to the $T_-\bar{T}_-$ process is $t\bar{t}$ production, whose production cross section with $E_{\mathrm{Tmiss}} >$ 400 GeV is $\mathcal{O}(10)$ or more times larger than the signal cross section. We study the E_{Tmiss} distribution as a function of M_{eff}. Because of a simple kinematic reason, the separation of the signal from background is best when $M_{\mathrm{eff}} \sim 2m_{T_-}$. A pseudoedge structure of the signal can be observed over the $t\bar{t}$ background in that region, and the significance of the signature turns out to be larger than 7σ for the case of $m_{T_-} \leq 900$ GeV.

The reconstructed signal is clearly different from that of SUSY events. In the case of SUSY, the production cross section of $\tilde{t}\tilde{t}^*$ is rather small and is not detectable. Scalar top quarks may be produced from gluino decay. In that case, additional jets are also produced, and the top cut $m_{\min}(jjj) < 200$ GeV for the jets in a hemisphere can hardly be satisfied.

Results of our simulation given in this paper should be regarded as an order of magnitude estimate. We have used the simple smearing and jet finding algorithms provided by the ACERDET code. The E_{Tmiss} and jet energy resolution could be different at the ATLAS and the CMS detectors in the LHC environment. Note that the energy resolution assumed by ACERDET is closer to the ATLAS detector [The default is $\Delta E/E = 50\%/\sqrt{E}$, while $\Delta E/E = 50\,(100)\%/\sqrt{E}$ for the ATLAS (CMS) detector]. Furthermore, the background from $t\bar{t}$ production is estimated by the HERWIG code in this paper, where $\sigma(t\bar{t}) =$ 400 pb. However, it is well known that the $t\bar{t}$ cross section receives large NLO corrections of around a factor of 2. The multijet final state $t\bar{t}$ + jets should also give an important background to the events with E_{Tmiss}. For the parameters we have studied, S/N is high in the signal region. Moreover, the signal has a peak structure in the E_{Tmiss} distribution. Therefore, we believe that our result is stable against additional sources of background and a factor of 2 increase of the background. In addition, $t\bar{t}$ production with a multijet final state has a better chance of having a large three jet invariant mass in a hemisphere, because events have additional jets which are not kinematically constrained by the top mass shell conditions. It is likely that the process $t\bar{t}$ + jets would be rejected by the top cut $m_{\min}(jjj) < 200$ GeV. It would be interesting to study the processes $t\bar{t}$ + jets and $T_-\bar{T}_-$ + jets to check this expectation explicitly.

In this paper, we do not study mass reconstruction in detail. The mass difference $m_{T_-} - m_{A_H}$ could be extracted from the $M_{\mathrm{eff}} - E_{\mathrm{Tmiss}}$ distribution if the background distribution can be calibrated precisely. We have also looked into the M_{T2} distribution for the sample with at least one reconstructed top quark, which shows positive correlation with the mass difference. The fit may be improved if the efficiency to reconstruct the top quark is improved by selecting the jets consistent with the top decay kinematics. The combinatorial backgrounds may be reduced if we select the top candidate among the jets in a hemisphere.

The existence of the top partner and dark matter associated with the T-parity symmetry is an important feature of physics beyond the standard model, as we discussed in the Introduction. The collider phenomenology of the top partner therefore deserves more realistic studies. We hope more realistic studies will be performed by the ATLAS and CMS groups in the future.

ACKNOWLEDGMENTS

This work is supported in part by the Grant-in-Aid for Science Research, Ministry of Education, Culture, Sports, Science and Technology, Japan (No. 16081211 for S. M., and No. 16081207 and No. 18340060 for M. M. N.).

[1] ATLAS Collaboration, *ATLAS Detector and Physics Performance Technical Design Report*, Report No. CERN-LHCC-99-14/15.

[2] CMS Collaboration, Physics TDR, Vol. I, Report No. CERN-LHCC-2006-0001, 2006; Physics TDR, Vol. II, Report No. CERN-LHCC-2006-0021, 2006.

[3] S. P. Martin, hep-ph/9709356.

[4] I. Hinchliffe, F. E. Paige, M. D. Shapiro, J. Soderqvist, and W. Yao, Phys. Rev. D **55**, 5520 (1997); H. Bachacou, I. Hinchliffe, and F. E. Paige, Phys. Rev. D **62**, 015009 (2000).

[5] N. Arkani-Hamed, A. G. Cohen, and H. Georgi, Phys. Lett. B **513**, 232 (2001); N. Arkani-Hamed, A. G. Cohen, E. Katz, A. E. Nelson, T. Gregoire, and J. G.

Wacker, J. High Energy Phys. 08 (**2002**) 021.
[6] N. Arkani-Hamed, A. G. Cohen, E. Katz, and A. E. Nelson, J. High Energy Phys. 07 (2002) 034.
[7] C. Csaki, J. Hubisz, G. D. Kribs, P. Meade, and J. Terning, Phys. Rev. D **67**, 115002 (2003); J. L. Hewett, F. J. Petriello, and T. G. Rizzo, J. High Energy Phys. 10 (2003) 062; C. Csaki, J. Hubisz, G. D. Kribs, P. Meade, and J. Terning, Phys. Rev. D **68**, 035009 (2003); T. Gregoire, D. R. Smith, and J. G. Wacker, Phys. Rev. D **69**, 115008 (2004); M. C. Chen and S. Dawson, Phys. Rev. D **70**, 015003 (2004); Z. Han and W. Skiba, Phys. Rev. D **72**, 035005 (2005); W. Kilian and J. Reuter, Phys. Rev. D **70**, 015004 (2004).
[8] H. C. Cheng and I. Low, J. High Energy Phys. 09 (2003) 051; 08 (2004) 061; I. Low, J. High Energy Phys. 10 (2004) 067.
[9] J. Hubisz and P. Meade, Phys. Rev. D **71**, 035016 (2005).
[10] M. Asano, S. Matsumoto, N. Okada, and Y. Okada, hep-ph/0602157.
[11] A. Birkedal, A. Noble, M. Perelstein, and A. Spray, Phys. Rev. D **74**, 035002 (2006).
[12] J. Hisano, K. Kawagoe, and M. M. Nojiri, Phys. Rev. D **68**, 035007 (2003).
[13] P. Meade and M. Reece, Phys. Rev. D **74**, 015010 (2006).
[14] M. Schmaltz and D. Tucker-Smith, Annu. Rev. Nucl. Part. Sci. **55**, 229 (2005); M. Perelstein, Prog. Part. Nucl. Phys. **58**, 247 (2007).
[15] G. Burdman, M. Perelstein, and A. Pierce, Phys. Rev. Lett. **90**, 241802 (2003); **92**, 049903(E) (2004); T. Han, H. E. Logan, B. McElrath, and L. T. Wang, Phys. Rev. D **67**, 095004 (2003); M. Perelstein, M. E. Peskin, and A. Pierce, Phys. Rev. D **69**, 075002 (2004).
[16] A. Belyaev, C. R. Chen, K. Tobe, and C. P. Yuan, Phys. Rev. D **74**, 115020 (2006).
[17] C. S. Chen, K. Cheung, and T. C. Yuan, Phys. Lett. B **644**, 158 (2007).
[18] D. N. Spergel *et al.* (WMAP Collaboration), Astrophys. J. Suppl. Ser. **148**, 175 (2003); C. L. Bennett *et al.*, Astrophys. J. Suppl. Ser. **148**, 1 (2003).
[19] J. Hubisz, P. Meade, A. Noble, and M. Perelstein, J. High Energy Phys. 01 (2006) 135.
[20] M. E. Peskin and T. Takeuchi, Phys. Rev. D **46**, 381 (1992).
[21] W. J. Marciano, hep-ph/0003181; M. Perelstein, M. E. Peskin, and A. Pierce, Phys. Rev. D **69**, 075002 (2004).
[22] ALEPH Collaboration, Phys. Rep. **427**, 257 (2006).
[23] CDF Collaboration, hep-ex/0507091.
[24] E. Boos *et al.* (CompHEP Collaboration), Nucl. Instrum. Methods Phys. Res., Sect. A **534**, 250 (2004).
[25] S. Kretzer, H. L. Lai, F. I. Olness, and W. K. Tung, Phys. Rev. D **69**, 114005 (2004).
[26] G. Corcella *et al.*, J. High Energy Phys. 01 (2001) 010.
[27] E. Richter-Was, hep-ph/0207355.
[28] F. Moortgat and L. Pape, CMS Physics TDR, Vol. II, Report No. CERN-LHCC-2006-021, 2006, Chap. 13.4, p. 410.
[29] P. Nason *et al.*, Nucl. Phys. **B303**, 607 (1988); M. Beneke *et al.*, hep-ph/0003033.
[30] S. Asai, in Proceedings of the 4th TEV4LHC, Fermilab, 2005, http://conferences.fnal.gov/tev4lhc/.
[31] A. Barr, C. Lester, and P. Stephens, J. Phys. G **29**, 2343 (2003).
[32] K. Kawagoe and M. M. Nojiri, Phys. Rev. D **74**, 115011 (2006).
[33] F. Moortgat, in Proceedings of SUSY06, 2006.